Materials Today Communications 30 (2022) 103033

Contents lists available at ScienceDirect

Materials Today Communications

journal homepage: www.elsevier.com/locate/mtcomm

Graphene-based materials behaviour for dyes adsorption

A. Paton-Carrero [a,*], P. Sanchez [a], L. Sánchez-Silva [a], A. Romero [a]

[a] University of Castilla-La Mancha, Department of Chemical Engineering, Avenida Camilo Jose Cela, 12 13071 Ciudad Real, Spain

ARTICLE INFO

Keywords:
graphene oxide
adsorption
dyes
functionalization

ABSTRACT

Due to the environmental damage caused by dye dumping, the scientific community has been researching into different adsorbents in order to mitigate this impact. In this respect, different graphene-based materials with a high adsorption capacity were studied (graphite and graphene oxide and two different types of reduced graphene oxide). In this work, four graphene-based materials with different properties and structures were evaluated. All materials were those obtained at each step in the pathway of oxidation, exfoliation, and reduction of graphite for conversion into reduced graphene. These four materials were characterized in depth by different methods (RAMAN, XRD, EDX, SEM, FTIR). Adsorption variables were researched to demonstrate their great adsorptive rate, which reached in some cases values of over 300 mg/g of adsorbed dye. Therefore, this study established a relationship between the physicochemical properties of the materials and their adsorption capacity. Furthermore, the effect of different variables on the process was studied: temperature, contact time and amount of adsorbent.This study creates new adsorbent materials with a long lifespan, reducing the environmental impact of industry on nature.

1. Introduction

Nowadays, many substances are discharged by industries and factories as liquid waste, or into the soil or atmosphere, which are harmful both to the environment and to human health. Discharge of these substances causes great environmental damage which is currently unsustainable, being one of the most important pollution by liquid effluents. Daily, water resources are contaminated by polluted which are highly detrimental to the environment and wildlife habitats [3] and dyes are some of the most harmful of these environmental pollutants Dyes can be defined as chemical compounds capable of connecting themselves to surfaces or fabrics in order to change their color [61]. Typically, these materials are complex organic molecules with great chemical stability due to their end use that requires them to resist reactive chemical agents such as detergents or bleaches [61]. In addition, dyes are used by a large number of industries: paper [21], textiles [23], food processing, cosmetic companies or plastics manufacturing, etc. [11,59]. Currently, there are more than 10,000 different types of dyes and it is estimated that at least 100 million tons of these compounds are produced annually, of which at least 15% end up in the hydrosphere (2014) [13]. This is not only detrimental to the environment, but also to human health. Studies have reported that dyes can be mutagenic and carcinogenic and may cause severe damage such as dysfunction of the kidneys, reproductive system, liver, brain, and central nervous system [47] Wastewater is an additional problem as, on average, 200 L of water are used to produce one kg of dye[41].

For all these reasons, not only dumped dyes must be removed, but also nonfixed ones that remain in liquid effluents must be reused. Despite the existence of numerous alternatives for removing these compounds, adsorption is the most effective treatment for mitigating pollution and water waste Several dye adsorbents have been studied so far. i.e.: activated bamboo [17], unburned carbon [58], bentonite [18], carbon nanotube [64], apricot seed [24], alumina [1], Fe_2O_3 [36].

Numerous studies support graphene-based materials asideal adsorbents for a large number of organic compounds [28,44,52,63]. In fact, the use of this material in water treatment is currently under investigation [8,36]. Studies suggest that the attractiveness of using graphene oxide for these molecules is mainly due to two important factors. First, the oxygenated groups on the structure generate electrostatic interactions and hydrogen bonds with the organic molecules. Second, the extensive surface area provides the material with many more active sites for adsorption of these compounds [62]. In addition, due to the high chemical stability and stable structure of graphene-based materials, it is possible to use them continuously in wastewater treatments by performing constant adsorption/desorption cycles without damaging the integrity of the material [60]. Another important factor in the use of

* Corresponding author.
E-mail address: AntonioPaton@uclm.es (A. Paton-Carrero).

https://doi.org/10.1016/j.mtcomm.2021.103033
Received 7 November 2021; Accepted 23 November 2021
Available online 27 November 2021

graphene-based materials as adsorbents is their high capacity of functionalization. This property enables complex molecules that produce more selective adsorption processes, or even chemical processes of adsorption and desorption of molecules, allowing to release substances while adsorbing pollutants [65]. All these properties make graphene-based materials a promising adsorbent for dye recovery.

The aim of this article was to study the adsorption capacity of two different dyes by using four graphene-based materials (graphite oxide, graphene oxide, chemical and thermal reduced graphene oxide) as adsorbents. These four materials had different structures and functional groups that could discern the effect that these properties had on adsorption. All the materials were completely characterized by different methods and the effect of different variables on the adsorption process was studied.

2. Experimental

2.1. Materials

Powder graphite (< 20 μm), hydrazine monohydrated (NH_2-NH_2) and acid red ($C_{18}H_{13}N_3Na_2O_8S_2$) were purchased from Sigma-Aldrich Chemistry®. Potassium permanganate ($KMnO_4$; purity >99%), sulphuric acid (H_2SO_4; 96%), hydrogen peroxide (H_2O_2; 110 vol.), hydrochloric acid (HCl; 5 N), ethanol (CH_3-CH_2OH; purity >99.5%) and methylene blue ($C_{16}H_{18}ClN_3S$) were purchased from Panreac®.

2.2. Synthesis of the adsorbents

2.2.1. Graphite and graphene oxide

Graphite was oxidized with an optimized Improved Hummers method [29] in which 15 g of graphite was mixed with 45 g of potassium permanganate and gradually added into 400 mL of sulphuric acid while the mixture was being vigorously stirred and kept at 50 ºC for 3 h. Afterwards, 3 mL of hydrogen peroxide was added to prevent oxidative reactions. Then, to reduce the temperature, 400 g of ice was mixed with the hydrogen peroxide. Next, this mixture was vacuum filtered. The cake obtained was then washed with 200 mL of water, 200 mL of ethanol and 200 mL of hydrochloric acid with filtering between each stage. The final mud was dried at 60ºC for 2 h in order to eliminate any residual ethanol. The product obtained was named GrO.

Graphene oxide was obtained by using the force of sound as a mechanical exfoliant. A water solution of 1 g per liter of graphite oxide was prepared and exfoliated with a sonicator. A sonotrode of stainless steel was placed in the liquid matrix during exfoliation with 1 cycle and 50% amplitude being the sonication parameters. The solution was sonicated for 2 h and the resulting solution was named GO. In order to characterize the material, the dry product had to be obtained by freeze-drying.

2.2.2. Reduced graphene oxide

Chemical reduction was carried out using hydrazine monohydrate as the reducing agent. In this reduction, 1 L of graphene oxide solution (1 g/L) was mixed with 1 mL of hydrazine monohydrated at 90 ºC for 3 h. Afterward, the mixture was vacuum filtered and washed with distilled water until a neutral pH of 7 was reached. The cake obtained was dried at 100ºC for 3 h and sieved [39]. The powder obtained was named CrGO.

Thermal reduction was carried out with a low-temperature stove in which the graphite oxide was reduced by heat, where there was a spontaneous reaction. The powder obtained was named TrGO.

2.3. Materials characterization

Infrared spectroscopy was measured with a SPECTRUM TWO spectrometer (Perkin Elmer, Inc) in an ATP module. Elemental analysis of the material was developed by EDX software installed in the Phenom ProX equipment where the SEM images were also captured. Raman spectra were performed with a SENTERRA spectrometer with a coupled 532 nm laser. X-ray spectra analysis were developed by the diffractometer PHILIPS, PW-1711 with CuKα radiation (λ = 0.15404 nm). The following crystallographic parameters were studied: crystal stack height (L_C), in-plane crystallite size or layer size (L_A), interlaminar space (d):

$$d = \frac{\lambda}{2\cdot \text{sen}\ \theta_1} \quad (1)$$

$$L_c = \frac{k_1\cdot\lambda}{FWHM\cdot cos\ \theta_1} \quad (2)$$

$$L_A = \frac{k_2\cdot\lambda}{FWHM\cdot cos\ \theta_2} \quad (3)$$

where:

K is radiation wavelength ($\lambda = 0.15404$ nm).

θ_1 is (0 0 2) diffraction peaks position (º).

θ_2 is (1 0 0) diffraction peaks position (º).

k_1 isform factor (k = 0.9).

k_2 isWarren form factor (k = 1.84).

FWHM is Full Width at Half Maximum of the corresponding diffraction peak (rad).

2.4. Methylene blue and acid red adsorption

Two 100 mg/L stock solution of methylene blue (MB) and acid red (AR) were prepared and diluted several times until the concentrations required in the experiments were reached. The adsorption isotherms were performed in 150 mL flasks with dye concentrations of 20 mg/L for each one. The graphene-based material solutions were prepared by pouring 2 g of dry material into 1 L of distillated water. Different amounts of graphene-based adsorbent (from 5 to 50 mg) were added to the flask while stirring. After different selected times, the adsorbent was separated by filtration. The final dye concentration was measured with a Pharma Spec 1700 Shimazu spectrophotometer. The effect of contact time was studied by stirring the solution for at least 12 h, measuring concentration several times. Adsorption temperature was studied by controlling temperature at 20,30, 40, 50 and 60 ºC. The total amount of dye adsorbed was calculated using Eq. 4:

$$q_e = \frac{(C_0 - C_e)}{m}\cdot V \quad (4)$$

where q_e is the adsorbed amount of dye (mg/g); C_0 and C_e are the initial and equilibrium concentrations of dye (mg/L), m is the mass of the adsorbent (g) and V is the volume of the solution (L).

Removal capacity of graphene-based material was calculated using the equation:

$$removal\quad (\%) = \frac{(C_0 - C_e)}{C_0}\cdot 100 \quad (5)$$

3. Results

3.1. Adsorbent characterization

Table 1 shows the elemental analysis corresponding to the studied

Table 1
Elemental analysis of the graphene-based adsorbents.

Material	C (%)	O (%)	Other* (%)	C/O
Graphite	100	0	–	–
GrO	50	45	5	1.12
GO	54	44	2	1.20
CrGO	69	21	10	3.28
TrGO	70	27	3	2.59

* elements such as K, Mn, Cl, N or S.

samples. The effectiveness of the oxidation process was shown with the graphite oxide structure 45 wt% for the oxygen groups. This quantity was fairly similar to that for the graphene oxide because exfoliation by sonication did not involve any chemical process and the chemical composition remained stable. Effective reduction for both pathways was also observed. The chemical one produced more reduced material with only 21% of oxygen groups remaining in the structure, whereas the thermal route produced a material with a higher amount of oxygen groups (27%).

Considering the C/O ratio, it is clear that although both reduced materials had similar percentages of oxygen, this ratio in the case of the chemically reduced material was higher than that for the thermally reduced one. This was not only due to the greater reduction in the oxygen functional groups, but also to the residual elements generated during chemical reduction (e.g. substituted nitrogen groups present in the structure) which were not present in the thermally reduced material.

FTIR analysis for all the samples was carried out (Fig. 1) in order to study the nature of the functional groups introduced after oxidation and, subsequently, relate them to the adsorption results.First, the FTIR spectrum for graphite does not show any visible functional groups due to the purity of the material which solely consists of carbon atoms. However, after oxidation and subsequent mechanical exfoliation, several oxygenated groups can be observed, which are the same in both oxides. The first observable peak between 3600 and 3000 cm^{-1}, was attributed to the O-H stretching vibrations of the hydroxyl groups [40]. Another related peak for the hydroxyl groups was located at 1450 cm^{-1} and in this case, it was related to the bending vibration of carboxylic acid groups attached to the edge of the structure. Carboxylic acid could also be detected in the C═O band, related to the stretching modes of the COOH groups located at 1750 cm^{-1} [6]. Another band was located at approximately 1630 cm^{-1} and was assigned to the C═C skeletal vibration of the graphene planes. The peak appearing at 1220–1230 cm^{-1} was attributed to the stretching vibration of the epoxy C-O-C group. The last band ranging from 1050 to 1100 cm^{-1} was ascribed to the alkoxy C-O stretching vibration [49].

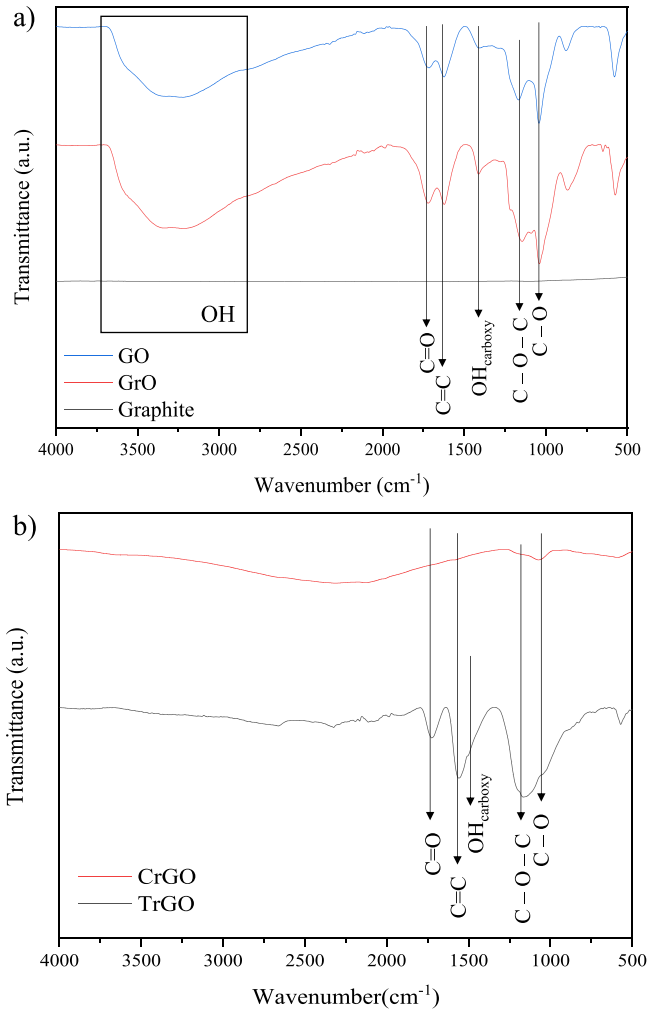

Fig. 1. FTIR spectra for the graphene-based materials. a) oxidized graphene-based materials; b) reduced graphene-based materials.

After both reduction processes, the removal of the oxygenated functional groups in the FTIR spectra of the samples is clearly observable. In both cases, the OH groups were completely removed, while other functional groups partially remained in the spectrum.

Focusing on chemical reduction, it is clear how practically all functional groups disappeared to show a virtually flattened spectrum. Only one band, corresponding to the C-O groups, can be clearly observed. The hydrazine reduction pathway primarily attacked epoxy groups, thus enabling the epoxy rings at the graphite edges to open, and this oxygen to be substituted with nitrogen groups anchored to the structure [12]. Although numerous studies have shown that hydrazine is a poor reducer for OH groups and their derivatives, calculations made by Kim et al. showed that hydroxyl groups can also be reduced by hydrazine, albeit greater energy is required. Therefore, reduction with hydrazine was very effective in reducing almost all the oxygenated functional groups [26].

The basis for removal of the functional groups in thermal reduction was the evolution of oxygenated molecules to CO and CO_2, by which empty spaces in the carbonaceous structure were generated. However, evolution to these molecules was thermally and kinetically limited by the amount and proximity of the oxygenated groups in the structure [51]. Recent studies have shown that temperatures above 1000 °C are needed for completely removing functional groups in the graphite oxide structure [27]. Low temperature elimination (< 200ºC) of a significant part of the oxygen functional groups in the GO structure, was aided by the high oxygen density of GrO [46]. However, by using this reduction method, the hydroxyl groups were largely removed and, other oxygenated functional groups such as C═O, C-O-C or C-O remained practically unaltered.

Finally, the thermal reduction procedure was less aggressive, with the C═C band clearly visible in the spectrum in sample TrGO. Opposite to this, during the chemical reduction, this band disappeared due to the structural attack that took place.

Raman is a characterization technique widely used for studying carbonaceous materials. Fig. 2 shows the Raman spectra for different adsorbents. It can be seen that in all cases, the Raman spectrum shows two peaks located at 1300 and 1500 cm^{-1}. The first one (~1350 cm^{-1}), called the D peak, corresponds with structural defects in the material. The second one (~1580 cm^{-1}), called the G peak, represents the graphical order of the carbonaceous samples. Finally, the 2D band, which appears around values of 2700 cm^{-1}, is defined as a second order band of the D-band and determine the number of layers of graphene in the samples [29].

In order to study these bands more exhaustively, the relationship between the intensities of the D and G peaks (I_D/I_G) was analyzed in detail. This ratio represents the amount of defects in the graphitic structure; the higher the ratio, more defects are present in the sample [45]. In this respect, it can be seen that graphite, being a crystalline material, has almost no structural defects ($I_D/I_G = 0.15$). Nevertheless, the trend after oxidation, exfoliation and reduction showed a rising number of defects due to the aggressiveness of the processes and after oxidation, in particular, the number of defects increased considerably ($I_D/I_G = 0.81$). Likewise, mechanical exfoliation using sound waves, despite not being a chemical treatment, slightly increased the number of defects ($I_D/I_G = 0.88$). This phenomenon might have been due to breakage of the graphene sheets and their separation after sonication. After chemical and thermal reduction, an increase in the ID/IG ratio with respect to the original material was observed as removing the

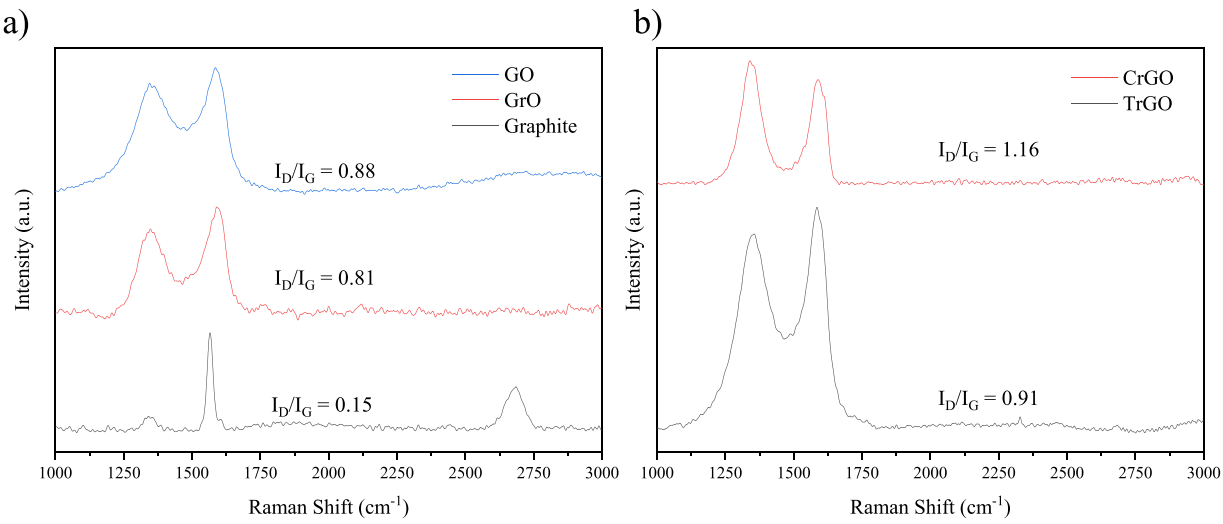

Fig. 2. Raman spectra of the graphene-based adsorbents. a) oxidized graphene-based materials; b) reduced graphene-based materials.

functional groups creates holes and defects in the carbonaceous structure and these were reflected in the Raman analysis. With chemical reduction this increase was even greater (I_D/I_G = 1.16) the increase observed in thermal reduction (I_D/I_G = 0.91) because it is a very aggressive chemical process with a high reduction capacity.

Furthermore, an increase in the width of the D and G bands was also observed in all cases after oxidation, exfoliation and reduction. This, as well as the slight shift in the bands to lower Raman shift values, was also indicative of the presence of structural defects not seen in the raw material [35].

The crystallographic nature of the graphene-based materials was also studied by X-ray diffraction. Table 2 shows the peak positions and the characteristic crystallographic variables of the materials. The (0 0 2) peak, located at 2θ ≈ 25 – 26°, corresponded to the aromatic stacking structure of the carbon layers on the (0 0 2) plane [53] while the (1 0 0) peak, located at 2θ, had to be close to 42°, indicated the orientation of the (1 0 0) planes on the graphene materials [43]. As observed, after graphite oxidation, the (0 0 2) peak was displaced to lower 2θ values. This was due to introducing functional groups into the graphite structure which modified the diffraction angle of the X-rays on striking the graphite surface. Likewise, the reduction process had the opposite effect on the displacement of peak (0 0 2). By removing the functional groups, the lightning diffraction returned to its original values and the peak moved back to the 2θ values observed before oxidation.

This displacement of the (002) peak lead to a change in the interlaminar space (d) in the material. For 2θ values close to 26°, this space was approximately 0.32 nm, while lower 2θ values (~10°) could correspond to spacings between 0.9 and 1 nm as a result of introducing oxygenated groups which caused the graphene sheets to separate. Nevertheless, the reduction process had the opposite effect. Thus, after reduction, the functional groups were removed from the graphite sheets, which made the C – C bonds reorder, thereby generating new interactions between the layers. This phenomenon again decreased the interlaminar space in the material and moved the (002) peak to higher 2θ values, thereby recovering values close to those in the original graphite. According to the crystalline size of the samples (L_A which represents layer size and L_C the stack height of the crystals) it can be seen that, as the physical-chemical processes of oxidation, exfoliation and reduction went underway, the value of both variables decreases. This was logical since in all the processes there was a great deal of destruction, as corroborated by the Raman characterization.

Table 2
XRD peak and crystallographic variables of the graphene-based adsorbents.

Sample	0 0 2 (°)	1 0 0 (°)	d (nm)	L_C (nm)	L_A (nm)
Graphite	26.62	–	0.32	37.1	–
GrO	9.91	42.48	0.89	5.08	10.38
GO	9.15	42.56	0.97	4.35	8.90
TrGO	23.24	42.88	0.38	2.18	4.46
CrGO	24.30	42.96	0.37	1.02	2.04

Fig. 3 shows SEM images of all samples. The SEM picture for graphite (Fig. 3a) shows perfectly ordered layers of material. After oxidation (Fig. 3b), morphological changes in the material are clearly observable. Oxidation produced a material with a more developed surface on which the oxidized graphene sheets formed reticulated graphite oxide amalgams. Fig. 3c. shows the appearance of the material after graphite oxide exfoliation. As can be seen, the graphene oxide flakes are perfectly separated; the edge of individual layers and a multiple lamellar layer structure can also clearly be observed [5]. Reduction processes lead to materials which are very different in structure. With TrGO (Fig. 3d), the structure obtained was similar to that of the original GrO only more developed, which gave rise to a more cotton-like appearance and this was attributed to the violent expansion of the material during reduction. With CrGO, reduction removed the oxygenated functional groups from the graphene oxide sheets very efficiently. This led to the appearance of new π – π bonds between the now free carbon atoms, followed by restacking of the graphite structures. The material shown in Fig. 3e, concerns more the graphene oxide structure but it seems that the graphite oxide sheets crumpled and formed a less laminar structure after the material restacked. This phenomenon was attributed to Van der Waals forces generated between the layers after reduction [2].

3.2. *Dye adsorption*

3.2.1. *Influence of adsorbent dose on dye adsorption*

Different adsorption experiments were carried out by varying the amount of adsorbent and calculating dye removal for each one. In methylene blue, MB, adsorption (Fig. 4a), it can be seen that an increase in dosage of the adsorbent leads to an increase in MB removal due to a rise in the surface area in contact with the dye, and this, in turn, increased the number of active sites for adsorption [15]. Theoretically, the graphene-based adsorbent coordinates with the MB molecule through the oxygen terminations (which were detected by FTIR) and the positive behavior of the final nitrogen groups in the MB structure [32]. Removal of MB in all the materials except CrGO reached almost 100% of the total amount of dye. With CrGO there was less adsorption, and only 30% of the MB in the solution was removed. This phenomenon may have been caused by the lower amount of oxygen groups and the more

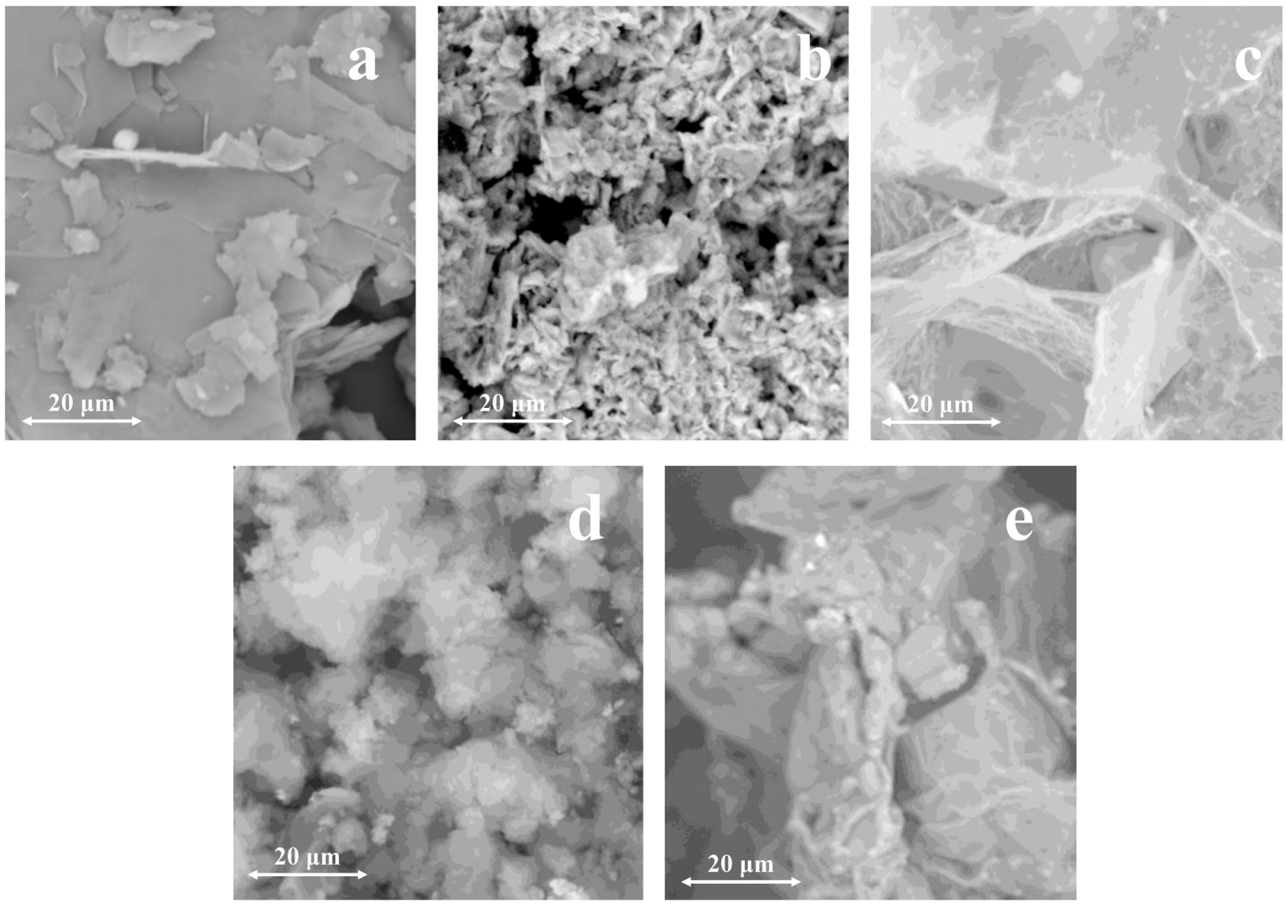

Fig. 3. SEM images. a) Graphite; b) GrO; c) GO; d) TrGO; e) CrGO.

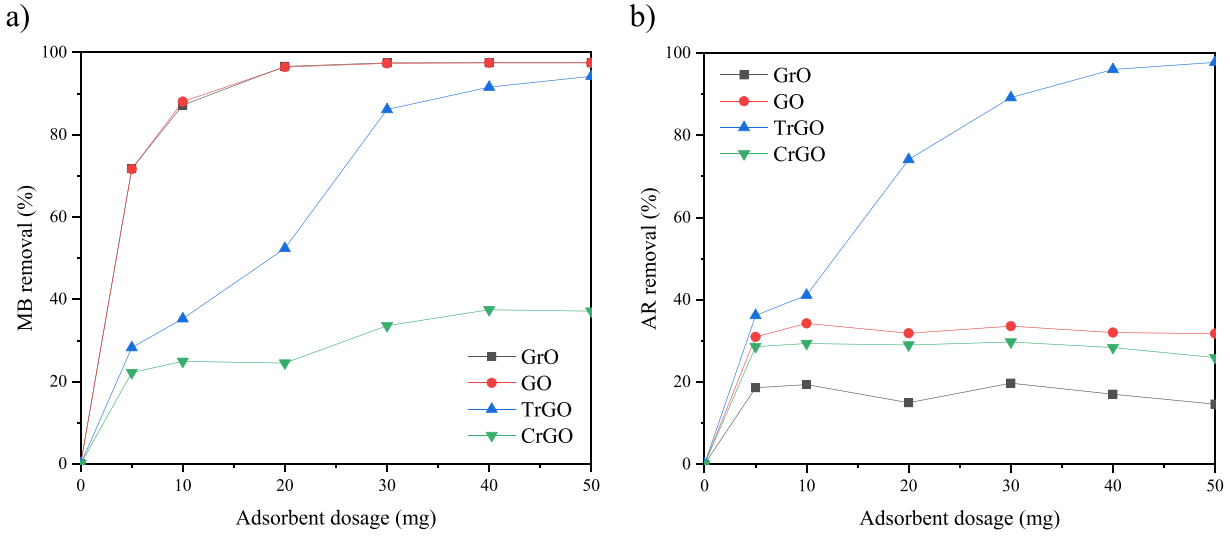

Fig. 4. Dye adsorption vs. adsorbent dose. a) methylene blue; b) acid red. (Room temperature, t = 180 min, C_0 = 30 ppm). (For interpretation of the references to colour in this figure legend, the reader is referred to the web version of this article.)

stacked structure which was related to the lower surface area.

With acid red adsorption (AR) (Fig. 4b), the adsorption trend was different to that seen with methylene blue. In this case, the best adsorbent was sample TrGO since it combined a low amount of oxygenated functional groups with a high surface area. The anionic AR dye (unlike the cationic MB) as well as the oxygenated functional groups were negatively charged. For this reason, RA adsorption was not favored by the adsorbents used as either they had a large number of oxygenated functional groups (GO, GrO) or a low surface area (CrGO). With TrGO, adsorption results were similar for both dyes since, in this material, the lower amount of oxygenated functional groups was combined with a high surface area. Finally, it should be stressed that RA adsorption was independent of the amount of adsorbent used (dosage > 5 mg) for all cases except in the TrGO sample. This may be due to the fact that an

increase in the amount of adsorbent produces, not only the appearance of aggregates, but also the sedimentation of adsorbent particles that reduces the active adsorption sites [16,38].

Based on the results obtained, a dose of 30 mg of adsorbent was selected as being the optimum one for adsorption. Lower doses did not enable complete adsorption in some cases.

3.2.2. *Influence of adsorbent-dye contact time on dye adsorption*

Fig. 5 shows total dye removal as a function of contact time. In almost all cases it can be observed that adsorption was immediate, with almost total adsorption reached during the first 10 min. However, with CrGO, for both dyes' adsorption required a little more time to reach equilibrium. This might have been linked to CrGO hydrophobia. After reducing the functional groups, the interaction between them and the water molecules decreased and the dispersibility of the material greatly decreased [4]. This statement can be concluded due to the fact that in all the cases the adsorption time was the same that the time required for a complete dispersion of graphene-based material in water For this reason, the time selected as being optimal was 120 min. This time was selected as, although most adsorption was immediate, CrGO needed more time to reach equilibrium. Thus, for purposes of accuracy, this time was used in the study.

3.2.3. *Adsorption equilibrium study*

The adsorption isotherms indicate the relationship between the adsorbent and the dye adsorbed at equilibrium. A mathematical analysis was performed in order to further analyze these isotherms. When observing adsorptive properties, two models are most widely used to represent equilibrium isotherms for carbonaceous materials: the Langmuir and Freundlich models. Langmuir (Eq. 6) is a model based on homogeneous monolayer adsorption on a homogeneous surface on which there are equivalent adsorption sites and energy throughout the surface [20].

$$\frac{C_e}{q_e} = \frac{1}{q_{max}} + \frac{C_e}{Q_m} \tag{6}$$

where q_{max} is the maximum adsorption capacity of the adsorbent (mg/g), and C_e and q_e are MB concentration in the solution (mg/l) and the adsorption capacity of GO (mg/g), respectively, at equilibrium.

In contrast, the Freundlich (Eq. 7) is an empirical model based on heterogeneous adsorption on a surface on which there are randomly located active sites producing non-homogeneous adsorption.[20].

$$\ln q_e = \ln k_f + \frac{1}{n} \cdot \ln C_e \tag{7}$$

where k_f is the Freundlich constant related to adsorption capacity (L/g) and n is an empirical parametre related to adsorption intensity.

Figs. 6 and 7 show the adsorption isotherms for MB and AR, respectively, at room temperature for each material. Langmuir and Freundlich adjustments are also represented.

A VBA-Excel application was developed to analyze the most important adsorption variables for each dye. The Marquardt–Levenberg algorithm was selected for the nonlinear regression procedure. The weighted sum of the squared differences between the observed and the calculated outlet flow rates was minimized [50] (Eq. 8).

$$SSQ = \sum_{I} \left(q_{e,th} - q_{e,exp}\right)^2 \tag{8}$$

where SSQ was the sum of square differences; $q_{e,th}$ and $q_{e,\ exp}$ denoted experimental and theoretical adsorption capacity, respectively.

An F-test is a statistical test in which the test statistic has an F-distribution under the null hypothesis. It is used for comparing statistical models that have been fitted to a data set, in order to identify the model that best fits the population from which the data were sampled.

The basis of the VBA-Excel application procedure was a comparison of the tabulated F value (F-test) and F_c, which is defined by Eq. 8.

$$F_c = \frac{\text{regression sum of squares/degree of freedom}}{\text{residual sum of squares / degrees of freedom}} = \frac{\sum_{i=1}^{N} \{[f(x,\beta)]_i^2 / p\}}{\sum_{i=1}^{N} \{[y - f(x,\beta)]_i^2 / (N-p)\}} \tag{9}$$

Note that if $F_c > F(p, N - p, 1 - \alpha)$ (assuming a value of $\alpha = 0.05$, 95% confidence level), the regression is considered to be meaningful, although this is no guarantee that the model is statistically suitable. To prevent this, the meaningfulness of the parameter in the model must also be evaluated by using the *t*-test, which verifies whether the estimation of $\beta_i(b_{fi})$ differs from a reference value (generally zero). Thus, a parameter will always be meaningful when inequation 10 is satisfied:

$$t_{Ci} = \frac{|b_{fi}|}{\sqrt{[V(b_f)]_{ii}}} > t\left(N - p; 1 - \frac{\alpha}{2}\right) \tag{10}$$

where $[V(b_f)]_{ii}$ represents the diagonal j_{th} term of the covariance matrix. Finally, the confidence interval of parametre β_{ii} is defined by Eq. 11:

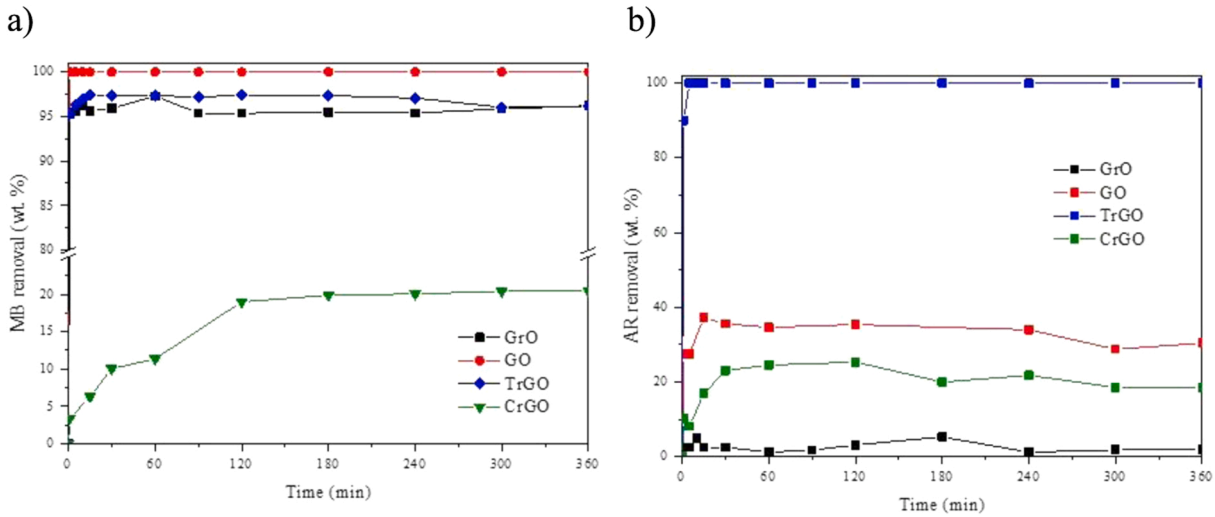

Fig. 5. Dye adsorption vs. contact time.*(room temperature, C_0= 30 ppm, m_{ads} = 30 mg).*

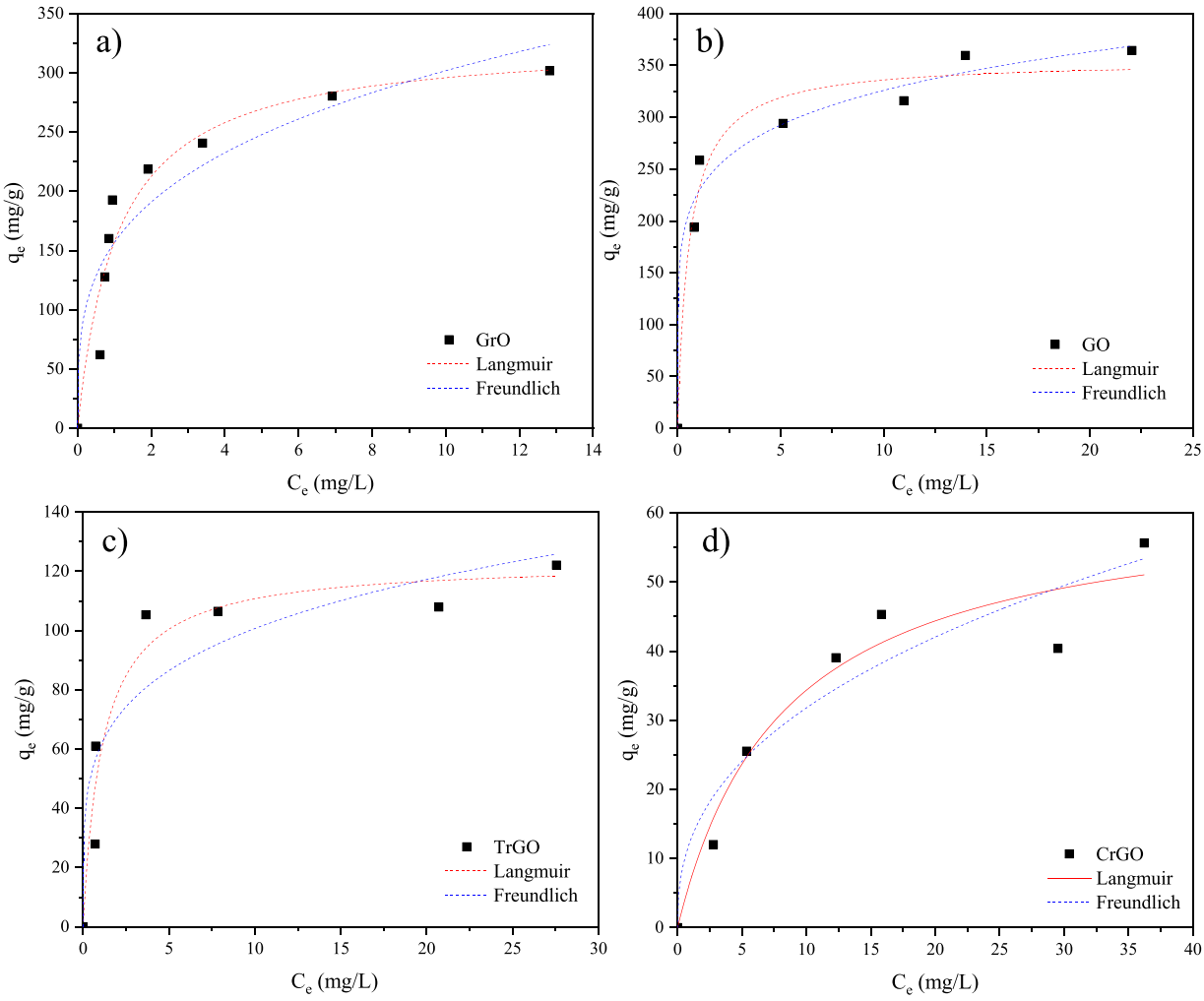

Fig. 6. Experimental adsorption isotherms of MB. Langmuir and Freundlich models (dotted lines). a) GrO; b) GO; c) TrGO; d) CrGO.(room temperature, t = 120 min, m_{ads} = 30 mg).

$$b_{fi} - t\left(N-p;1-\frac{\alpha}{2}\right)\sqrt{\left[V\left(b_f\right)\right]_{ii}} \le \beta_j \le b_{fi} + t\left(N-p;1-\frac{\alpha}{2}\right)\sqrt{\left[V\left(b_f\right)\right]_{ii}} \quad (11)$$

where F_C is the function defined by Eq. 8; t_c is the function defined by Eq. 9; b is the estimate of β; V(b) is the covariance matrix; N is the total number of experiments; x is the set of independent variables in f(x,β) mode; y is the experimental dependent variable; f is the (x,β) mathematical model; and p is the number of parameters in a model.

In order to select the best adsorption model, Pearsonś chi-squared test (χ2) was performed. This test establishes whether an observed frequency distribution differs from a theoretical one. The higher the χ2 value (Eq. 12), the less plausible the null hypothesis is (which assumes equality in both distributions) [42]. Thus, the lower the values of χ2, the better fit the model is. Table 3 and Table 4 show the adsorption and statistical parametres for both dyes.

$$\chi^2 = \sum_i \left[\frac{\left(q_{e,th}-q_{e,exp}\right)^2\left(observed_i - theoretical_i\right)^2}{q_{e,th}theoretical_i}\right]_i \quad (12)$$

Considering the results obtained, it may be inferred that, for all materials and dyes, the best fitting adsorption model was the Langmuir one. This model was based on the premise of single-cup adsorption that has homogenous, active sites throughout the entire surface [31]. However, there is one exception to this: with MB adsorption, graphene oxide fits somewhat better in Freundlich's experimental model. This could be due to the fact that after exfoliation of the material, a greater number of functional groups could be exposed because as the surface area increased the mathematical model increasingly favored the experimental model to the theoretical one [28]. Focusing on MB adsorption, adsorption capacity was as follows: GO>GrO>TrGO>CrGO with graphene oxide being the material with highest adsorption capacity, which reached 355 mg/g. As for AR, the trend for the materials was as follows: TrGO>CrGO>GO>GrO where TrGO was the material with the highest adsorption capacity, which reached 123 mg/g.

For purposes of comparison, Table 5 shows the maximum adsorption capacity of the different adsorbent materials for both dyes. It can be seen that with methylene blue the capacity achieved in this study was clearly higher or closer to the value reported in the literature. However, with red acid, this was much lower than that found in the literature. This might have been because with acid red adsorption, follow-up treatment is necessary in order to introduce functional groups capable of generating active sites for the adsorption of acid dyes. However, this was not necessary for methylene blue because the functional groups generated after oxidation could generate the active sites that enabled adsorption of basic dyes.

3.2.4. *Influence of temperature on dye adsorption*

The effect of temperature on adsorption was studied, while simultaneously calculating some dependent variables. Due to the low

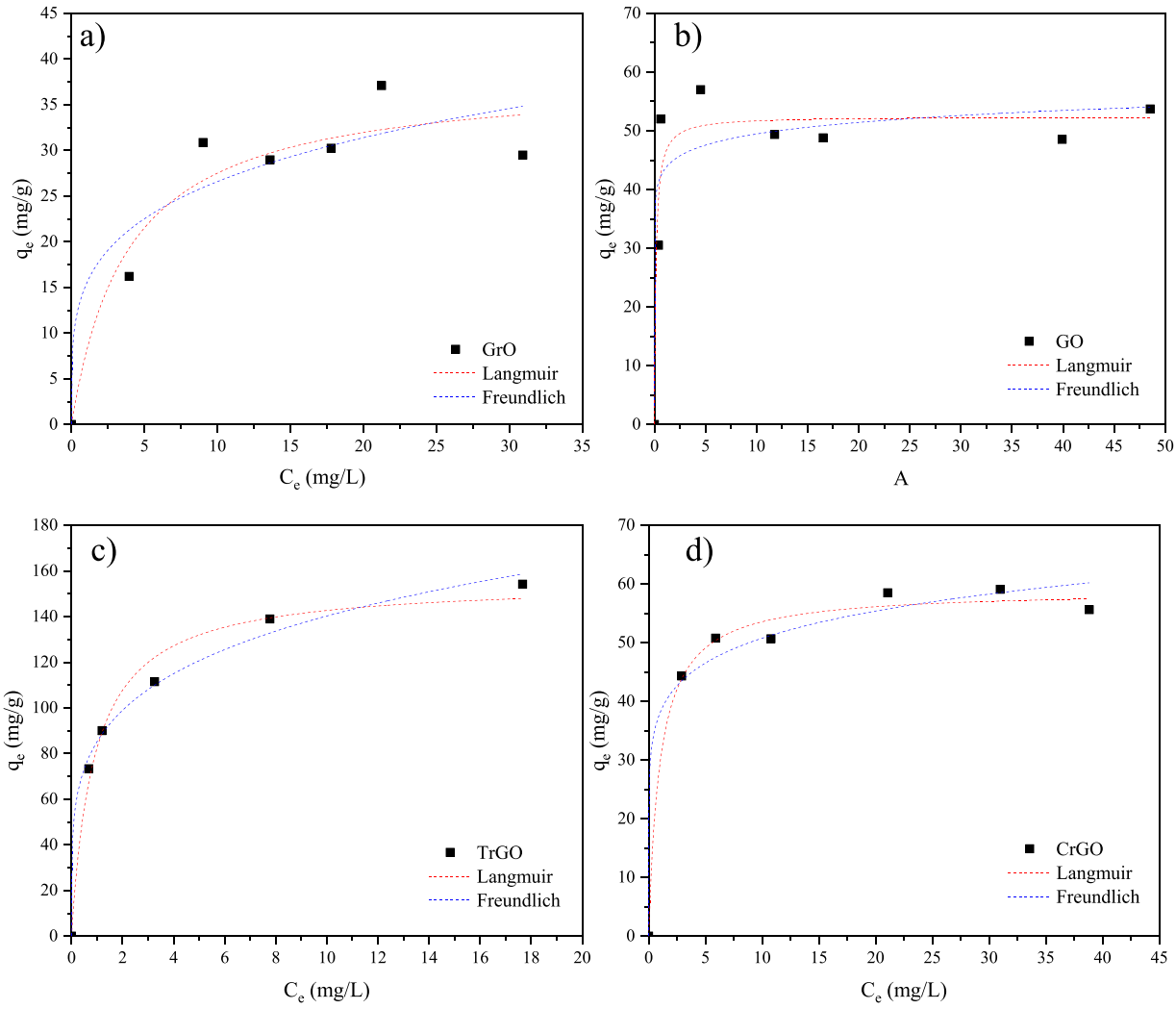

Fig. 7. Experimental adsorption isotherms of AR at room temperature. Langmuir and Freundlich models (dotted lines). a) GrO; b) GO; c) TrGO; d) CrGO. (room temperature, t = 120 min, m_{ads} = 30 mg).

Table 3
Parameters and statistical values calculated by the Marquardt-Lavenberg algorithm for MB adsorption.

SAMPLE	MODEL	PARAMETER	VALUE	t_c	t_{test}	t_c/t_{test}	STATISTICAL SIGNIFICANCE	χ^2
GrO	Langmuir	q_{max} (mg/g)	327.99	12.74	2.57	4.96	YES	5151
	Freundlich	k_f (L/g)	156.74	10.21	2.57	3.97	YES	9163
		N	3.51	5.05	2.57	1.96	YES	
GO	Langmuir	q_{max} (mg/g)	354.84	24.12	2.57	9.39	YES	2722
	Freundlich	k_f (L/g)	227.52	17.57	2.57	6.84	YES	2012
		N	6.4	6.38	2.57	2.48	YES	
TrGO	Langmuir	q_{max} (mg/g)	123.32	13.93	2.57	5.42	YES	746
	Freundlich	k_f (L/g)	60.72	5.76	2.57	2.24	YES	1661
		n	4.55	2.57	2.57	1.00	YES	
CrGO	Langmuir	q_{max} (mg/g)	62.68	7.81	2.57	3.04	YES	129
	Freundlich	k_f (l/g)	12.57	3.29	2.57	1.28	YES	201
		n	2.48	4.11	2.57	1.60	YES	

adsorption capacity of the acid dye, only methylene blue was studied to avoid errors. In this study, different temperatures in the range 303–323 °C were used. Thermodynamic variables were calculated using the following equations [34]:

$$\ln K_0 = \frac{\Delta S^0}{R} - \frac{\Delta H^0}{R \cdot T} \quad (13)$$

where ΔS^0 was change in entropy during the process (J/mol·K), ΔH^0 was change in enthalpy during the process (J/mol), R was the universal gas constant (8.314 J/mol·K), T was current temperature (K) and K_0 was the distribution coefficient which could be obtained from the slope of $\ln(q_e/C_e)$ versus q_e [55]. In addition, ΔG^0, the free Gibbs energy (J/mol) was calculated as follow [57]:

$$\ln K_0 = -\frac{\Delta G^0}{R \cdot T} \quad (14)$$

Table 6 shows the ΔS^0, ΔH^0, ΔG^0 values obtained for the above equations. Looking at these, the positive entropy (ΔS^0) values indicated

Table 4
Parameters and statistical values calculated by the Marquardt-Lavenberg algorithm for AR adsorption.

SAMPLE	MODEL	PARAMETER	VALUE	t_c	t_{test}	t_c/t_{test}	STATISTICAL SIGNIFICANCE	χ^2
GrO	Langmuir	q_{max} (mg/g)	38.05	8.42	2.57	3.28	YES	70
	Freundlich	k_f (l/g)	27.93	9.73	2.57	3.79	YES	104
		n	4.22	2.17	2.57	0.84	NO	
GO	Langmuir	q_{max} (mg/g)	54.67	10.8	2.57	4.20	YES	69
	Freundlich	k_f (l/g)	46.94	8.80	2.57	3.42	YES	89
		n	2.18	1.34	2.57	0.52	NO	
TrGO	Langmuir	q_{max} (mg/g)	155.28	28.36	2.57	11.04	YES	186
	Freundlich	k_f (L/g)	85.15	33.30	2.57	12.96	YES	189
		n	4.61	15.05	2.57	5.86	YES	
CrGO	Langmuir	q_{max} (mg/g)	58.99	27.74	2.57	10.79	YES	45
	Freundlich	k_f (L/g)	38.37	14.94	2.57	5.81	YES	53
		n	8.5	5.01	2.57	1.95	YES	

Table 5
Recently reported adsorption capacities for different adsorbent materials.

Adsorbents	Dye	Adsorption Capacity	Sources
Activated carbon	MB	149.3	[22]
rGO/TNT	MB	26.3	[37]
MCNT	MB	43.8	[57]
Modified biomass	MB	109.9	[7]
Zeolite/chitosan	MB	199.7	[25]
GO	MB	243.9	[30]
NMCN-3	AR	221.22	[19]
CeO2.xH20	AR	540.2	[56]
Polisilicates	AR	304.8	[33]
Chitosan hydrogel	AR	565.1	[48]
PU/chitosan	AR	267.2	[10]
Ppy/SRM/GO	AR	294.1	[14]

Table 6
Thermodynamic parametres for removing MB on all materials.

MATERIAL	ΔG^0 (J/mol)			ΔH^0 (kJ/mol)	ΔS^0 (kJ/mol·K)
	303.15 K	313.15 K	323.15 K		
GrO	-4939,1	-4940,47	-5084,55	-2,74	12,63
GO	-4958,69	-5211,77	-5252,38	-1,12	7,15
TrGO	-4686,06	-4331,88	-3630,11	-20,66	52,7
CrGO	-4239,06	-4085,48	-3948,16	-22,29	59,22

good affinity of all materials for methylene blue, as well as an increase in the randomness of the solid-dissolution interface [57]. Similarly, negative values for enthalpy (ΔH^0) suggested that adsorption was exothermic [54]. In addition, the enthalpy values could determine the type of adsorption that was carried out: values under 20 kJ/mol showed a process dominated by physisorption, whereas between 20 and 80 kJ/mol this was dominated by both physisorption and chemisorption, and for values over 80 kJ/mol, chemisorption [31]. In this study, despite obtaining values very close to the border, all adsorption processes might have been dominated by physisorption of the dye in the adsorbent matrix. Negative ΔG^0 values indicate spontaneous processes, which showed, in turn our methylene blue adsorption occurred without any external agent acting [9]. However, the trend for ΔG^0 showing an increase in temperature proved to be different for each adsorbent. With oxidized and exfoliated materials (GO and GrO), the ΔG^0 values were more negative, which might indicate that adsorption equilibrium increases with temperature. However, with the reduced materials (TrGO and CrGO) the inverse was true: the equilibrium of the reaction was higher, the lower the temperature in the experiment was [57].

4. Conclusions

In this study, four different graphene-based materials (graphite, graphene and two different reduced graphene oxides) were studied as adsorbents for two types of dyes: methylene blue and acid red. Exhaustive characterization enabled us to study the effect different physicochemical treatments had on the materials and their adsorption capacities. In this study, the combination of surface area and functional group was seen to have a significant effect on dye adsorption. In all cases, this was immediate. According to the adsorption isotherms, almost all materials fit the Langmuir model, except for graphene oxide for methylene blue which fits the Freundlich experimental one. With methylene blue adsorption, graphene oxide was the material with the highest adsorption capacity (354.84 mg/g) while for acid red adsorption, thermally reduced graphene oxide was that with the best capacity (155.28 mg/g). After this study, it was concluded that the optimal conditions to obtain these adsorption values were 30 mg of adsorbent and 120 min of contact time. The thermodynamic study showed that the methylene blue adsorption process was dominated by physisorption, was spontaneous and there was high adsorbent-dissolution affinity. In addition, this study showed that the adsorptive capacities of graphite and graphene oxide were higher when temperature increased, whereas in both reduced materials, these capacities were lower when this happened.

CRediT authorship contribution statement

A. Patón designed and performed the experiments, characterized the samples and analyzed the data. **A. Romero and A. Patón** wrote the manuscript with support from **P. Sanchez. L. Sánchez-Silva** helped supervise the project. **A. Romero and A. Patón** conceived the original idea.

Declaration of Competing Interest

The authors declare that they have no known competing financial interests or personal relationships that could have appeared to influence the work reported in this paper.

Acknowledgments

The authors wish to thank the Spanish company Graphenano Nanotechnologies (UCTR16017) for their financial support. This research was also supported by the "Junta de Comunidades de Castilla-La Mancha (JCCM)" and European Union FEDER funds (SBPLY/180501/000281).

References

[1] A. Adak, M. Bandyopadhyay, A. Pal, Removal of crystal violet dye from wastewater by surfactant-modified alumina, Sep. Purif. Technol. 44 (2) (2005) 139–144.
[2] N.C. Adak, et al., Effects of hydrazine reduced graphene oxide on the inter-laminar fracture toughness of woven carbon fiber/epoxy composite, Compos. Part B: Eng. 149 (2018) 22–30.
[3] A. Ahmad, et al., Recent advances in new generation dye removal technologies: novel search for approaches to reprocess wastewater, RSC Adv. 5 (39) (2015) 30801–30818.

[4] H.S. Ahn, J.M. Kim, M.H. Kim, Experimental study of the effect of a reduced graphene oxide coating on critical heat flux enhancement, Int. J. Heat. Mass Transf. 60 (2013) 763–771.
[5] S.N. Alam, N. Sharma, L. Kumar, Synthesis of graphene oxide (GO) by modified hummers method and its thermal reduction to obtain reduced graphene oxide (rGO), Graphene 6 (1) (2017) 1–18.
[6] A. Alazmi, et al., Comparative study of synthesis and reduction methods for graphene oxide, Polyhedron 116 (2016) 153–161.
[7] M.E. Argun, et al., Activation of pine cone using Fenton oxidation for Cd(II) and Pb (II) removal, Bioresour. Technol. 99 (18) (2008) 8691–8698.
[8] de Assis, L.K., et al., Adsorption capacity comparison between graphene oxide and graphene nanoplatelets for the removal of coloured textile dyes from wastewater. Environmental technology, 2019.
[9] G. Crini, Kinetic and equilibrium studies on the removal of cationic dyes from aqueous solution by adsorption onto a cyclodextrin polymer, Dyes Pigments 77 (2) (2008) 415–426.
[10] R. da Rosa Schio, et al., Synthesis of a bio–based polyurethane/chitosan composite foam using ricinoleic acid for the adsorption of Food Red 17 dye, Int. J. Biol. Macromol. 121 (2019) 373–380.
[11] S. Dawood, T.K. Sen, C. Phan, Synthesis and characterisation of novel-activated carbon from waste biomass pine cone and its application in the removal of congo red dye from aqueous solution by adsorption, Water, Air, Soil Pollut. 225 (1) (2013) 1818.
[12] L. Dong, et al., Synthesis and reduction of large sized graphene oxide sheets, Chem. Soc. Rev. 46 (23) (2017) 7306–7316.
[13] R. Dutta, et al., Ultrafast removal of cationic dye using agrowaste-derived mesoporous adsorbent, Ind. Eng. Chem. Res. 53 (48) (2014) 18558–18567.
[14] S. Ebrahimpoor, et al., Bees metaheuristic algorithm with the aid of artificial neural networks for optimization of acid red 27 dye adsorption onto novel polypyrrole/SrFe12O19/graphene oxide nanocomposite, Polym. Bull. 76 (12) (2019) 6529–6553.
[15] E.N. El Qada, Allen S.J, Walker G.M, Adsorption of Basic Dyes onto Activated, Carbon Using Micro Ind. Eng. Chem. Res. 45 (17) (2006) 6044–6049.
[16] A. Fakhri, Adsorption characteristics of graphene oxide as a solid adsorbent for aniline removal from aqueous solutions: Kinetics, thermodynamics and mechanism studies, J. Saudi Chem. Soc. 21 (2017) S52–S57.
[17] B.H. Hameed, A.T.M. Din, A.L. Ahmad, Adsorption of methylene blue onto bamboo-based activated carbon: Kinetics and equilibrium studies, J. Hazard. Mater. 141 (3) (2007) 819–825.
[18] S. Hong, et al., Adsorption thermodynamics of Methylene Blue onto bentonite, J. Hazard. Mater. 167 (1) (2009) 630–633.
[19] T. Hu, et al., Engineering of rich nitrogen-doped and magnetic mesoporous carbon nanospheres with predictable size uniformity for acid dye molecules adsorption, Microporous Mesoporous Mater. 279 (2019) 234–244.
[20] Y. Huang, et al., Preparation of porous graphene/carbon nanotube composite and adsorption mechanism of methylene blue, SN Appl. Sci. 1 (1) (2019) 37.
[21] K. Ivanov, et al., Possibilities of using zeolite as filler and carrier for dyestuffs in paper, Papier 50 (7–8) (1996) 456–460.
[22] A.H. Jawad, et al., Adsorption of methylene blue onto activated carbon developed from biomass waste by H2SO4 activation: kinetic, equilibrium and thermodynamic studies, Desalin. Water Treat. 57 (52) (2016) 25194–25206.
[23] I. Kabdaşli, O. Tünay, D. Orhon, Wastewater control and management in a leather tanning district, Water Sci. Technol. 40 (1) (1999) 261–267.
[24] S. Kahraman, P. Yalcin, H. Kahraman, The evaluation of low-cost biosorbents for removal of an azo dye from aqueous solution, Water Environ. J. 26 (3) (2012) 399–404.
[25] W.A. Khanday, M. Asif, B.H. Hameed, Cross-linked beads of activated oil palm ash zeolite/chitosan composite as a bio-adsorbent for the removal of methylene blue and acid blue 29 dyes, Int. J. Biol. Macromol. 95 (2017) 895–902.
[26] M.C. Kim, G.S. Hwang, R.S. Ruoff, Epoxide reduction with hydrazine on graphene: A first principles study, J. Chem. Phys. 131 (6) (2009), 064704.
[27] M. Lavin-Lopez, et al., Influence of the reduction strategy in the synthesis of reduced graphene oxide, Adv. Powder Technol. 28 (12) (2017) 3195–3203.
[28] M. Lavin-Lopez, et al., The influence of graphite particle size on the synthesis of graphene-based materials and their adsorption capacity, Colloids Surf. A: Physicochem. Eng. Asp. 582 (2019), 123935.
[29] Md Lavin-Lopez, P., et al, Influ. Differ. Improv. Hummers Method. Modif. Charact. Graph. oxide Order Make a more easily scalable Method. Ind. Eng. Chem. Res. 55 (50) (2016) 12836–12847.
[30] Y. Li, et al., Comparative study of methylene blue dye adsorption onto activated carbon, graphene oxide, and carbon nanotubes, Chem. Eng. Res. Des. 91 (2) (2013) 361–368.
[31] J.Y. Lim, et al., Recent trends in the synthesis of graphene and graphene oxide based nanomaterials for removal of heavy metals — A review, J. Ind. Eng. Chem. 66 (2018) 29–44.
[32] A. Molla, et al., Selective adsorption of organic dyes on graphene oxide: Theoretical and experimental analysis, Appl. Surf. Sci. 464 (2019) 170–177.
[33] A.S.O. Moscofian, et al., Organofunctionalized magnesium phyllosilicates as mono- or bifunctitonal entities for industrial dyes removal, RSC Adv. 2 (8) (2012) 3502–3511.
[34] G. Moussavi, R. Khosravi, The removal of cationic dyes from aqueous solutions by adsorption onto pistachio hull waste, Chem. Eng. Res. Des. 89 (10) (2011) 2182–2189.
[35] R. Muzyka, et al., Characterization of Graphite Oxide and Reduced Graphene Oxide Obtained from Different Graphite Precursors and Oxidized by Different Methods Using Raman Spectroscopy, Materials 11 (7) (2018) 1050.
[36] N.N. Nassar, Kinetics, mechanistic, equilibrium, and thermodynamic studies on the adsorption of acid red dye from wastewater by γ-fe2o3 nanoadsorbents, Sep. Sci. Technol. 45 (8) (2010) 1092–1103.
[37] C.H. Nguyen, R.-S. Juang, Efficient removal of methylene blue dye by a hybrid adsorption–photocatalysis process using reduced graphene oxide/titanate nanotube composites for water reuse, J. Ind. Eng. Chem. 76 (2019) 296–309.
[38] K.S. Padmavathy, G. Madhu, P.V. Haseena, A study on Effects of pH, Adsorbent Dosage, Time, Initial Concentration and Adsorption Isotherm Study for the Removal of Hexavalent Chromium (Cr (VI)) from Wastewater by Magnetite Nanoparticles. Procedia, Technology 24 (2016) 585–594.
[39] S. Park, et al., Hydrazine-reduction of graphite-and graphene oxide, Carbon 49 (9) (2011) 3019–3023.
[40] A. Paton-Carrero, et al., Influence of the oxidizing agent in the synthesis of graphite oxide, J. Mater. Sci. (2020) 55.
[41] A.R. Petcu, et al., Nonionic microemulsion systems applied for removal of ionic dyes mixtures from textile industry wastewaters, Sep. Purif. Technol. 158 (2016) 155–159.
[42] R.L. Plackett, Karl Pearson and the Chi-Squared Test, Int. Stat. Rev. 51 (1) (1983) 59–72.
[43] O.Y. Podyacheva, et al., Nitrogen doped carbon nanotubes and nanofibers: Composition, structure, electrical conductivity and capacity properties, Carbon 122 (2017) 475–483.
[44] G.K. Ramesha, et al., Graphene and graphene oxide as effective adsorbents toward anionic and cationic dyes, J. Colloid Interface Sci. 361 (1) (2011) 270–277.
[45] A. Romero, et al., Comparative study of different scalable routes to synthesize graphene oxide and reduced graphene oxide, Mater. Chem. Phys. 203 (2018) 284–292.
[46] A. Romero, et al., Different strategies to simultaneously N-doping and reduce graphene oxide for electrocatalytic applications, J. Electroanal. Chem. 857 (2020), 113695.
[47] M.A.M. Salleh, et al., Cationic and anionic dye adsorption by agricultural solid wastes: A comprehensive review, Desalination 280 (1) (2011) 1–13.
[48] M. Salzano de Luna, et al., Chitosan hydrogels embedding hyper-crosslinked polymer particles as reusable broad-spectrum adsorbents for dye removal, Carbohydr. Polym. 177 (2017) 347–354.
[49] G. Shao, et al., Graphene oxide: the mechanisms of oxidation and exfoliation, J. Mater. Sci. 47 (10) (2012) 4400–4409.
[50] Z. Sihaib, et al., Manganese oxide-based catalysts for toluene oxidation, Appl. Catal. B: Environ. 209 (2017) 689–700.
[51] C. Sun, et al., Solvothermally exfoliated fluorographene for high-performance lithium primary batteries, Nanoscale 6 (5) (2014) 2634–2641.
[52] Y. Sun, et al., Interaction between Eu(III) and Graphene Oxide Nanosheets Investigated by Batch and Extended X-ray Absorption Fine Structure Spectroscopy and by Modeling Techniques, Environ. Sci. Technol. 46 (11) (2012) 6020–6027.
[53] H. Takagi, et al., XRD analysis of carbon stacking structure in coal during heat treatment, Fuel 83 (17) (2004) 2427–2433.
[54] H. Teng, C.-T. Hsieh, Influence of surface characteristics on liquid-phase adsorption of phenol by activated carbons prepared from bituminous Coal, Ind. Eng. Chem. Res. 37 (9) (1998) 3618–3624.
[55] W.T. Tsai, et al., Adsorption of ethyl violet dye in aqueous solution by regenerated spent bleaching earth, J. Colloid Interface Sci. 289 (2) (2005) 333–338.
[56] H. Wang, et al., High-efficiency adsorption for acid dyes over CeO2·xH2O synthesized by a facile method, J. Alloy. Compd. 776 (2019) 96–104.
[57] P. Wang, et al., Kinetics and thermodynamics of adsorption of methylene blue by a magnetic graphene-carbon nanotube composite, Appl. Surf. Sci. 290 (2014) 116–124.
[58] S. Wang, et al., Unburned carbon as a low-cost adsorbent for treatment of methylene blue-containing wastewater, J. Colloid Interface Sci. 292 (2) (2005) 336–343.
[59] D. Wróbel, A. Boguta, R.M. Ion, Mixtures of synthetic organic dyes in a photoelectrochemical cell, J. Photochem. Photobiol. A: Chem. 138 (1) (2001) 7–22.
[60] W. Wu, et al., Highly efficient removal of Cu(ii) from aqueous solution by using graphene oxide, Water, Air, Soil Pollut. 224 (1) (2012) 1372.
[61] M.T. Yagub, et al., Dye and its removal from aqueous solution by adsorption: a review, Adv. Colloid Interface Sci. 209 (2014) 172–184.
[62] H. Yan, et al., Effects of the oxidation degree of graphene oxide on the adsorption of methylene blue, J. Hazard. Mater. 268 (2014) 191–198.
[63] Z. Yang, et al., Flocculation performance and mechanism of graphene oxide for removal of various contaminants from water, Water Res. 47 (9) (2013) 3037–3046.
[64] Y. Yao, et al., Adsorption behavior of methylene blue on carbon nanotubes, Bioresour. Technol. 101 (9) (2010) 3040–3046.
[65] M. Zaboli, et al., Probing the adsorption and release mechanisms of cytarabine anticancer drug on/from dopamine functionalized graphene oxide as a highly efficient drug delivery system, J. Mol. Liq. 301 (2020), 112458.